

Supporting Information

**NaMoO₃(IO₃)(H₂O): Water Molecule Introduction Induces
Strong Second Harmonic Generation Response, Widened
Band Gap and Large Anisotropy.**

Contents

Table S1. Atomic coordinates ($\times 10^4$), equivalent isotropic displacement parameters ($\text{\AA}^2 \times 10^3$) and BVS for $\text{NaMoO}_3(\text{IO}_3)(\text{H}_2\text{O})$	3
Table S2. Bond lengths (\AA) for $\text{NaMoO}_3(\text{IO}_3)(\text{H}_2\text{O})$	4
Table S3. Band gap and birefringence data for some representative inorganic oxide optical crystals.....	5
Table S4. The calculated dipole moments of anionic groups within a unit cell of $\text{NaMoO}_3(\text{IO}_3)(\text{H}_2\text{O})$	6
Table S5. Calculated SHG coefficients of $\text{NaMoO}_3(\text{IO}_3)(\text{H}_2\text{O})$	7
Figure S1. The calculated (Dark Cyan) and experimental (The colors orange and LT Magenta represent fresh samples and samples exposed to humid air for more than 3 months, respectively) powder X-ray diffraction patterns of $\text{NaMoO}_3(\text{IO}_3)(\text{H}_2\text{O})$	8
Figure S2. EDS analysis of $\text{NaMoO}_3(\text{IO}_3)(\text{H}_2\text{O})$	8
Figure S3. The coordination environment of Na atoms in the structure of $\text{NaMoO}_3(\text{IO}_3)(\text{H}_2\text{O})$	9
Figure S4. The Na-O line consisted by $[\text{Na}(1)\text{O}_7]$ polyhedra.....	9
Figure S5. The connection mode of $[\text{MoO}_6]$ octahedra and $[\text{IO}_3]$ pyramids within the structures of $\text{AMoO}_3(\text{IO}_3)$ ($\text{A} = \text{NH}_4^+$ and alkali-metal ions) family.....	9
Figure S6. The comparison of layer orientation and distance within the structures of $\text{NaMoO}_3(\text{IO}_3)(\text{H}_2\text{O})$ and $\alpha\text{-KMoO}_3(\text{IO}_3)$	10
Figure S7. The degree of torsion for adjacent $[\text{MoO}_6]$ octahedron in Mo-O chain for $\text{NaMoO}_3(\text{IO}_3)(\text{H}_2\text{O})$ and $\alpha\text{-KMoO}_3(\text{IO}_3)$	10
Figure S8. The different dihedral angle between two $[\text{IO}_3]$ groups in $\text{NaMoO}_3(\text{IO}_3)(\text{H}_2\text{O})$ and $\alpha\text{-KMoO}_3(\text{IO}_3)$	10
Figure S9. Infrared spectrum of $\text{NaMoO}_3(\text{IO}_3)(\text{H}_2\text{O})$	11
Figure S10. TG and DSC curves of $\text{NaMoO}_3(\text{IO}_3)(\text{H}_2\text{O})$	11
Figure S11. The powder X-ray diffraction patterns of the intermediate after calcination at 300 °C of $\text{NaMoO}_3(\text{IO}_3)(\text{H}_2\text{O})$	12
Figure S12. The powder X-ray diffraction patterns of the residue after calcination at 600 °C of $\text{NaMoO}_3(\text{IO}_3)(\text{H}_2\text{O})$	12

Table S1. Atomic coordinates ($\times 10^4$), equivalent isotropic displacement parameters ($\text{\AA}^2 \times 10^3$) and BVS for $\text{NaMoO}_3(\text{IO}_3)(\text{H}_2\text{O})$.

	x	y	z	U(eq)	BVS
I(1)	5189(2)	2668(3)	3298(2)	12(1)	5.00
I(2)	4794(2)	7669(3)	3198(2)	12(1)	5.38
Mo(1)	7678(3)	4999(3)	5652(4)	7(1)	6.14
Mo(2)	2306(3)	9980(3)	4339(4)	7(1)	6.18
Na(1)	7505(15)	-190(30)	6000(20)	47(6)	0.98
Na(2)	2479(16)	4690(30)	4690(20)	41(5)	1.01
O(1)	8870(20)	30(30)	3740(40)	23(6)	-
O(2)	1120(20)	4940(30)	6840(40)	27(6)	-
O(3)	5990(30)	600(40)	3420(30)	28(7)	1.93
O(4)	3830(20)	2110(30)	4200(30)	20(5)	2.28
O(5)	5960(20)	3420(30)	5600(30)	17(5)	2.27
O(6)	8630(20)	3320(30)	6260(30)	22(5)	1.86
O(7)	7240(20)	5620(30)	8050(30)	15(5)	1.82
O(8)	8700(20)	6610(30)	5580(40)	32(6)	1.88
O(9)	6110(20)	7120(30)	4680(40)	27(6)	2.58
O(10)	3980(30)	5640(30)	2870(40)	31(7)	2.01
O(11)	4020(20)	8420(30)	5150(30)	21(5)	1.88
O(12)	1360(20)	8290(30)	4480(30)	24(6)	1.85
O(13)	1280(20)	11600(30)	3780(40)	28(6)	1.86
O(14)	2760(20)	9460(30)	1940(30)	12(5)	1.88

Table S2. Bond lengths (Å) for NaMoO₃(IO₃)(H₂O)

bond	length	bond	length
I(1)-O(3)	1.83(3)	Na(1)-O(1)	2.40(3)
I(1)-O(4)	1.77(2)	Na(1)-O(1)#5	2.30(3)
I(1)-O(5)	1.84(2)	Na(1)-O(3)#5	2.62(3)
I(2)-O(9)	1.70(3)	Na(1)-O(3)	2.37(3)
I(2)-O(10)	1.81(3)	Na(1)-O(6)	2.99(3)
I(2)-O(11)	1.86(2)	Na(1)-O(8)#6	2.85(3)
Mo(1)-O(5)	2.24(2)	Na(1)-O(9)#6	2.68(3)
Mo(1)-O(6)	1.68(3)	Na(2)-O(2)#1	2.36(3)
Mo(1)-O(7)	1.95(2)	Na(2)-O(2)	2.33(3)
Mo(1)-O(7)#1	1.94(2)	Na(2)-O(4)	2.56(3)
Mo(1)-O(8)	1.68(3)	Na(2)-O(10)#7	2.62(3)
Mo(1)-O(9)	2.40(2)	Na(2)-O(10)	2.39(4)
Mo(2)-O(4)#2	2.36(2)	Na(2)-O(13)#6	2.77(3)
Mo(2)-O(11)	2.23(2)	O(1)-H(1A)	0.97
Mo(2)-O(12)	1.68(2)	O(1)-H(1B)	0.97
Mo(2)-O(13)	1.69(2)	O(2)-H(2A)	0.97
Mo(2)-O(14)	1.93(2)	O(2)-H(2B)	0.97

Symmetry transformations used to generate equivalent atoms: #1 $x, -y+1, z-1/2$ #2 $x, y+1, z$ #5
 $x, -y, z+1/2$ #6 $x, y-1, z$ #7 $x, -y+1, z+1/2$

Table S3. Band gap and birefringence data for some representative inorganic oxide optical crystals.

	Crystal	Band		Ref.
		gap (eV)	Birefringence	
	$\text{NH}_4\text{MoO}_3(\text{IO}_3)$	3.26	0.083 @1064 nm ^{cal}	1
	$\gamma\text{-KMoO}_3(\text{IO}_3)$	3.30	0.087 @1064 nm ^{cal}	2
	$\text{KRb}[(\text{MoO}_3)_2(\text{IO}_3)_2]$	3.32	0.146 @1064 nm ^{cal}	1
Alkali metal molybdenum iodate family crystals	$\text{LiMoO}_3(\text{IO}_3)$	2.80	0.178 @1064 nm ^{cal}	3
	$\text{Cs}_2\text{MoO}_2\text{F}_3(\text{IO}_2\text{F}_2)$	3.31	0.204 @1064 nm ^{cal}	4
	$\text{NaMoO}_3(\text{IO}_3)$	3.19	0.208 @1064 nm ^{cal}	2
	$\text{Rb}_2\text{MoO}_2\text{F}_3(\text{IO}_2\text{F}_2)$	3.33	0.217 @1064 nm ^{cal}	4
	$\text{AMoO}_3(\text{IO}_3)$ (A= K, Rb, Cs)	3.10	-	5
	$\delta\text{-KMoO}_3(\text{IO}_3)$	3.34	-	6
	A few commercial crystals	BaB_2O_4		0.122 @532 nm ^{exp}
YVO_4			0.204 @532 nm ^{exp}	8
CaCO_3			0.172 @532 nm ^{exp}	9
$\epsilon\text{-La}(\text{IO}_3)_3$			0.0295 @visible light ^{exp}	10
A few iodate crystals	$\text{K}_2\text{Zn}(\text{IO}_3)_3(\text{I}_2\text{O}_5(\text{OH}))(\text{IO}_2(\text{OH}))(\text{H}_2\text{O})$		0.054 @visible light ^{exp}	11
	$\text{Ce}(\text{IO}_3)_4$		0.052 @546 nm ^{exp}	12
	$\text{CeF}_2(\text{IO}_3)_2$		0.212 @546nm ^{exp}	12
This work	$\text{NaMoO}_3(\text{IO}_3)(\text{H}_2\text{O})$	3.44	0.231 @visible light^{exp}	

Table S4. The calculated dipole moments of anionic groups within a unit cell of NaMoO₃(IO₃)(H₂O).

Polar unit (a unit cell)	Symmetric operation	Dipole moment (D)			
		<i>x</i>	<i>y</i>	<i>z</i>	total
I(1)O ₃	x, y, z	-2.7502	-8.5311	13.1336	15.9008
I(1)O ₃	x, 1-y, 0.5+z	-2.7486	8.5315	13.1321	15.8994
I(2)O ₃	x, 1-y, 0.5+z	-0.0127	9.8102	14.1248	17.1974
I(2)O ₃	x, y, z	-0.0134	-9.8106	14.1224	17.1956
Net dipole moment (IO ₃)		-5.5249	0	54.5129	54.7921
Mo(1)O ₆	x, 1-y, -0.5+z	-3.6865	-1.0223	-0.9718	3.9471
Mo(1)O ₆	x, y, z	-3.6878	1.0207	-0.9730	3.9482
Mo(2)O ₆	x, -1+y, z	4.3588	1.4927	0.9377	4.7017
Mo(2)O ₆	x, 1-y, 0.5+z	4.3580	-1.4933	0.9390	4.7014
Net dipole moment (MoO ₆)		1.3424	0	-0.0681	1.3442
Net dipole moment		-4.1825	0	54.4447	54.6052
Cell volume (Å ³)		610.87 (9)			
Dipole moment density		54.6052 / 610.87 = 0.0893 D Å ⁻³			
Dipole moment density (IO ₃)		54.7921 / 610.87 = 0.0897 D Å ⁻³			

Table S5. Calculated SHG coefficients of NaMoO₃(IO₃)(H₂O).

SHG tensor components	Values (pm/V)	SHG tensor components	Values (pm/V)
d_{111}	-0.24	d_{133}	-0.31
d_{112}	0	d_{222}	0
d_{113}	-0.89	d_{223}	-0.38
d_{122}	-0.32	d_{233}	0
d_{123}	0	d_{333}	-2.29

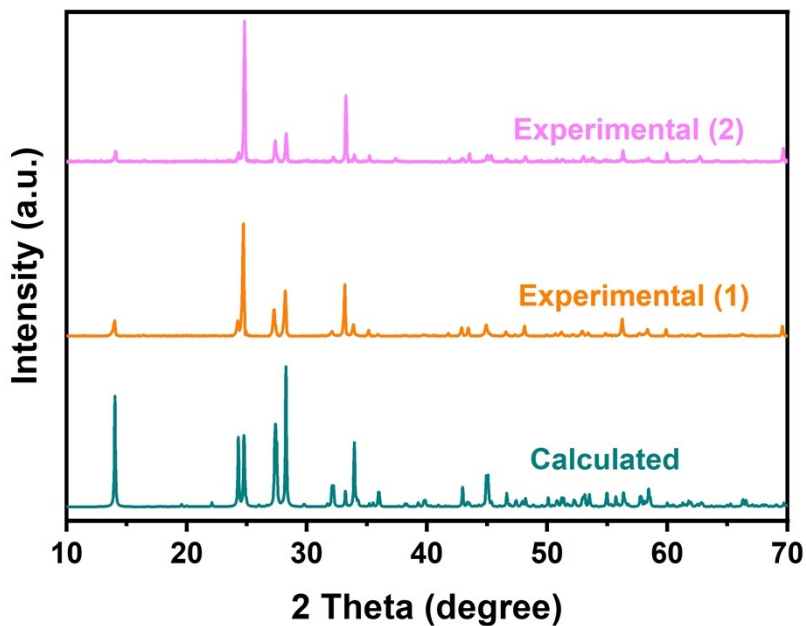


Figure S1. The calculated (Dark Cyan) and experimental (The colors orange and LT Magenta represent fresh samples and samples exposed to humid air for more than 3 months, respectively) powder X-ray diffraction patterns of $\text{NaMoO}_3(\text{IO}_3)(\text{H}_2\text{O})$.

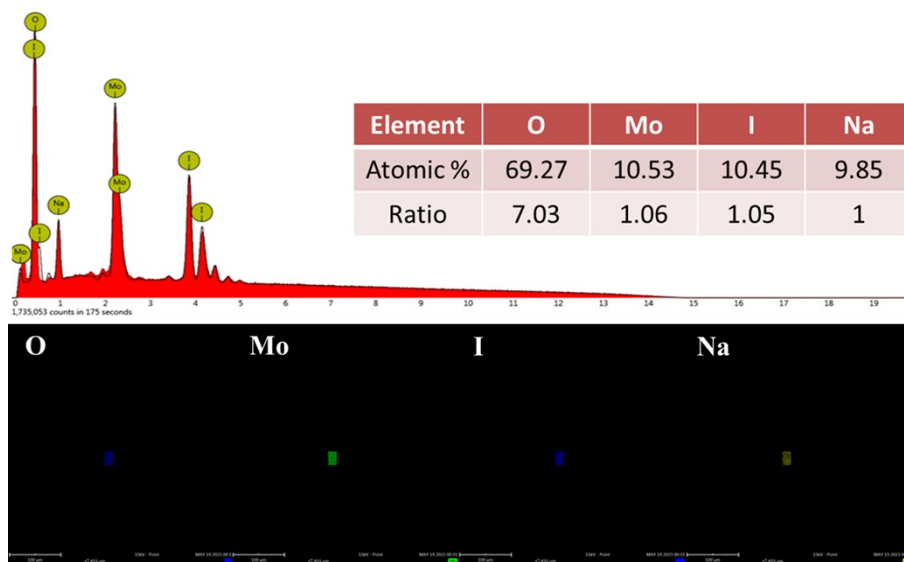


Figure S2. EDS analysis of $\text{NaMoO}_3(\text{IO}_3)(\text{H}_2\text{O})$.

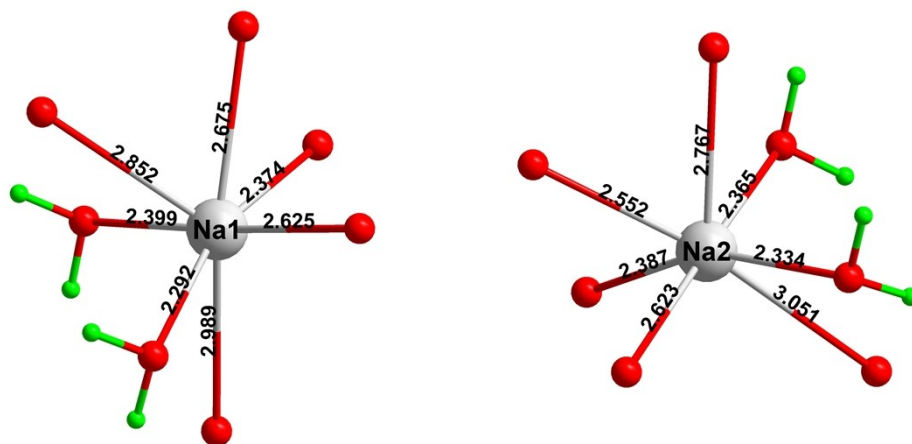


Figure S3. The coordination environment of Na atoms in the structure of $\text{NaMoO}_3(\text{IO}_3)(\text{H}_2\text{O})$

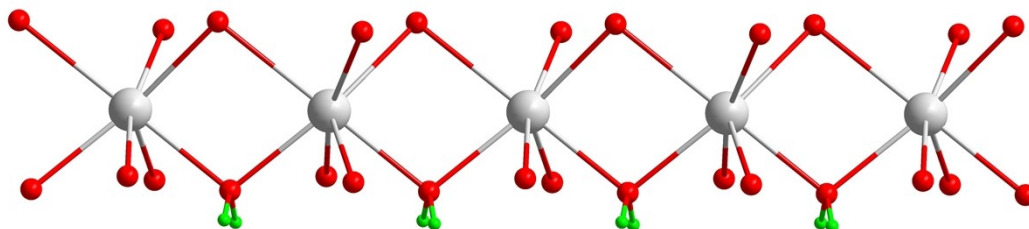


Figure S4. The Na-O line consisted by $[\text{Na}(1)\text{O}_7]$ polyhedra.

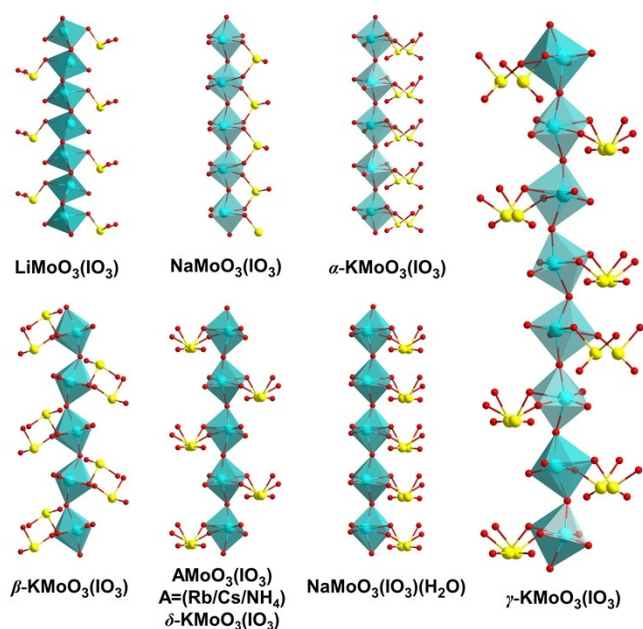


Figure S5. The connection mode of $[\text{MoO}_6]$ octahedra and $[\text{IO}_3]$ pyramids within the structures of $\text{AMoO}_3(\text{IO}_3)$ ($\text{A} = \text{NH}_4^+$ and alkali-metal ions) family.

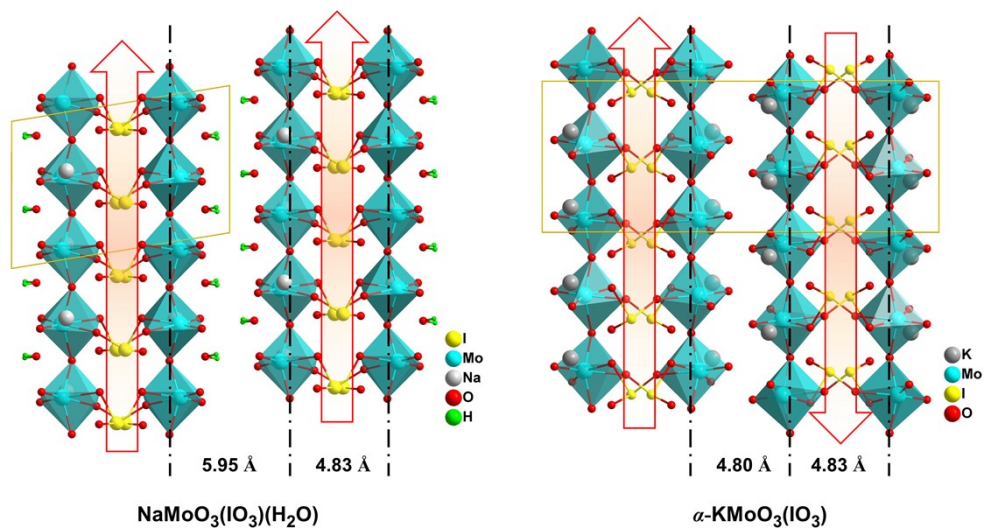


Figure S6. The comparison of layer orientation and distance within the structures of NaMoO₃(IO₃)(H₂O) and *α*-KMoO₃(IO₃).

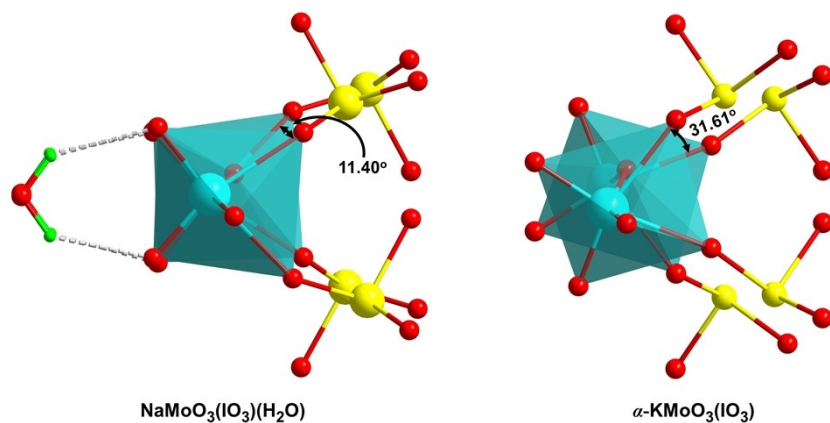


Figure S7. The degree of torsion for adjacent [MoO₆] octahedron in Mo-O chain for NaMoO₃(IO₃)(H₂O) and *α*-KMoO₃(IO₃).

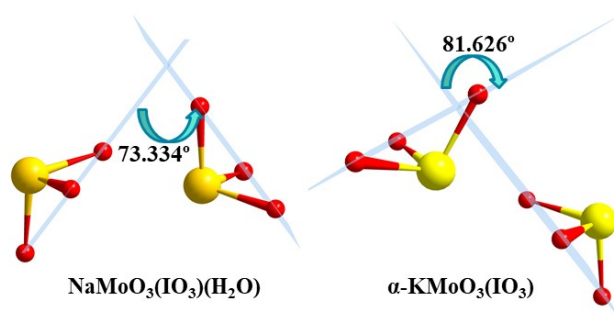


Figure S8. The different dihedral angle between two [IO₃] groups in NaMoO₃(IO₃)(H₂O) and *α*-KMoO₃(IO₃).

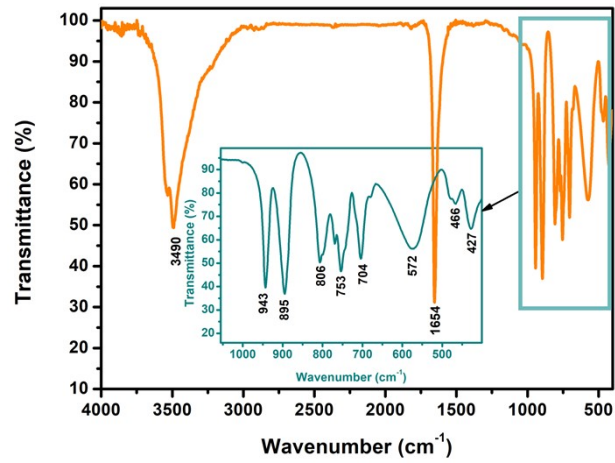


Figure S9. Infrared spectrum of $\text{NaMoO}_3(\text{IO}_3)(\text{H}_2\text{O})$.

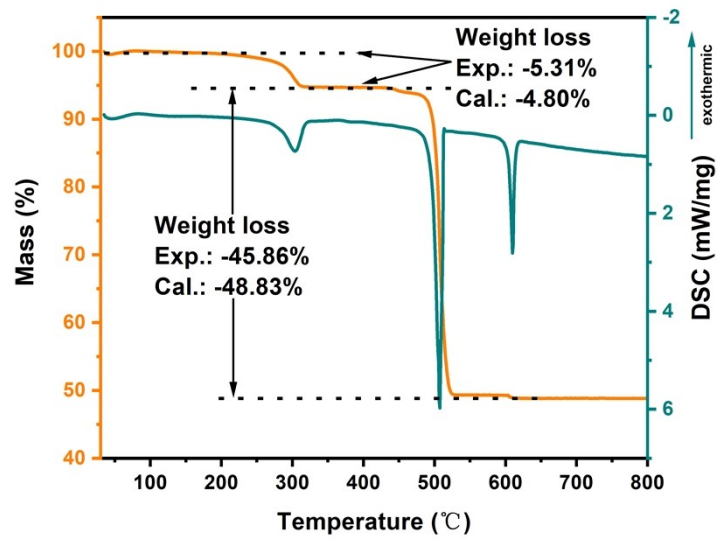


Figure S10. TG and DSC curves of $\text{NaMoO}_3(\text{IO}_3)(\text{H}_2\text{O})$.

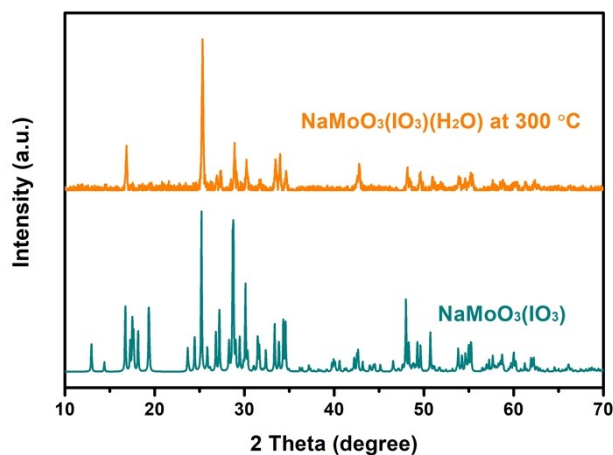


Figure S11. The powder X-ray diffraction patterns of the intermediate after calcination at 300 °C of $\text{NaMoO}_3(\text{IO}_3)(\text{H}_2\text{O})$.

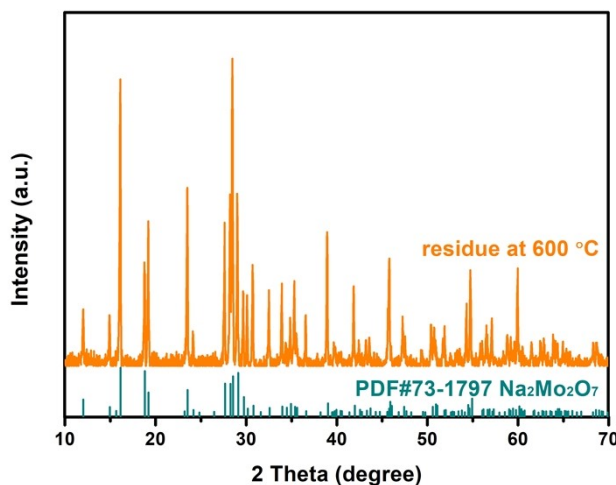


Figure S12. The powder X-ray diffraction patterns of the residue after calcination at 600 °C of $\text{NaMoO}_3(\text{IO}_3)(\text{H}_2\text{O})$.

Notes and references

- 1 Y. Li, G. Han, H. Yu, H. Li, Z. Yang and S. Pan, Two polar molybdenum(VI) iodates(V) with large second-harmonic generation responses, *Chem. Mater.*, 2019, **31**, 2992-3000.
- 2 J. Chen, C. Hu, Y. Li, Q. Chen, B. Li and J. Mao, $\text{AMoO}_3(\text{IO}_3)$ (A = Na and K): two promising optical materials via properly assembling the A-shaped basic building units, *J. Alloys Compd.*, 2022, **894**, 162547.
- 3 X. Chen, L. Zhang, X. Chang, H. Xue, H. Zang, W. Xiao, X. Song and H. Yan, $\text{LiMoO}_3(\text{IO}_3)$: a new molybdenyl iodate based on WO_3 -type sheets with large SHG response, *J. Alloys Compd.*, 2007, **428**, 54-58.
- 4 Y. Hu, X. Jiang, C. Wu, Z. Huang, Z. Lin, M. G. Humphrey and C. Zhang, $\text{A}_2\text{MoO}_2\text{F}_3(\text{IO}_2\text{F}_2)$ (A = Rb, Cs): strong nonlinear optical responses and enlarged band gaps through fluorine incorporation, *Chem. Mater.*, 2021, **33**,

- 5700-5708.
- 5 R. E. Sykora, K. M. Ok, P. S. Halasyamani and T. E. Albrecht-Schmitt, Structural modulation of molybdenyl iodate architectures by alkali metal cations in $\text{AMoO}_3(\text{IO}_3)$ (A = K, Rb, Cs): a facile route to new polar materials with large SHG responses, *J. Am. Chem. Soc.*, 2002, **124**, 1951-1957.
 - 6 Q. Li, H. N. Liu, H. W. Yu, Z. G. Hu, J. Y. Wang, Y. C. Wu, and H. P. Wu, Alignment of Λ -shaped basic building units to construct one new $\text{KMoO}_3(\text{IO}_3)$ polar polymorph, *Inorg. Chem.*, 2023, **62**, 3896-3903.
 - 7 G. Zhou, J. Xu, X. Chen, H. Zhong, S. Wang, K. Xu, P. Deng, F. Gan, P. Deng and F. Gan, Growth and spectrum of a novel birefringent α - BaB_2O_4 crystal, *J. Cryst. Growth*, 1998, **191**, 517-519.
 - 8 H. T. Luo, T. Tkaczyk, E. L. Dereniak, K. Oka and R. Sampson, High birefringence of the yttrium vanadate crystal in the middle wavelength infrared, *Opt. Lett.*, 2006, **31**, 616-618.
 - 9 G. Ghosh, Dispersion-equation coefficients for the refractive index and birefringence of calcite and quartz crystals, *Opt. Commun.*, 1999, **163**, 95-102.
 - 10 D. Wang, X. Zhang, P. Gong, Z. Lin, Z. Hu and Y. Wu, ϵ - $\text{La}(\text{IO}_3)_3$: a polar iodate with high thermal stability and a large second-harmonic-generation response obtained by a supercritical hydrothermal method, *Inorg. Chem.*, 2023, **62**, 6565-6569.
 - 11 J. Chen, P. Yang, H. Yu, Z. Hu, J. Wang, Y. Wu and H. Wu, Designing a strong second-harmonic generation polar iodate by the structure-directing properties of the “Tumbler-like” $[\text{Zn}(\text{IO}_3)(\text{I}_2\text{O}_5(\text{OH}))]$ polyanions, *ACS Mater. Lett.*, 2023, 1665-1671.
 - 12 T. Wu, X. Jiang, C. Wu, H. Sha, Z. Wang, Z. Lin, Z. Huang, X. Long, M. G. Humphrey and C. Zhang, From $\text{Ce}(\text{IO}_3)_4$ to $\text{CeF}_2(\text{IO}_3)_2$: fluorinated homovalent substitution simultaneously enhances SHG response and bandgap for mid-infrared nonlinear optics, *J. Mater. Chem. C*, 2021, **9**, 8987-8993.